Ab Initio Kinetic Simulation of Gas-Phase Experiments: Tautomerization of Cytosine and Guanine

ARTICLE *in* THE JOURNAL OF PHYSICAL CHEMISTRY B · MAY 2009

Impact Factor: 3.3 · DOI: 10.1021/jp810570w · Source: PubMed

7 AUTHORS, INCLUDING:

Dmytro Kosenkov
Monmouth University
23 PUBLICATIONS **388** CITATIONS
SEE PROFILE

Oleg V Shishkin
National Academy of Sciences of Ukraine
842 PUBLICATIONS **4,920** CITATIONS
SEE PROFILE

Dmytro Mykolayovych Hovorun
National Academy of Sciences of Ukraine
379 PUBLICATIONS **2,053** CITATIONS
SEE PROFILE

Michel Mons
Atomic Energy and Alternative Energies Co…
130 PUBLICATIONS **3,229** CITATIONS
SEE PROFILE

Ab Initio Kinetic Simulation of Gas-Phase Experiments: Tautomerization of Cytosine and Guanine

Dmytro Kosenkov,[†] Yana Kholod,[†] Leonid Gorb,[†,‡] Oleg Shishkin,[§] Dmytro M. Hovorun,[‡] Michel Mons,[∥] and Jerzy Leszczynski*[,†]

Interdisciplinary Center for Nanotoxicity, Department of Chemistry, Jackson State University, Jackson, Mississippi 39217, Department of Molecular and Quantum Biophysics, Institute of Molecular Biology and Genetics, National Academy of Sciences of Ukraine, 150 Zabolotnoho vul., Kyiv 03143, Ukraine, STC "Institute for Single Crystals", National Academy of Sciences of Ukraine, Kharkiv 61001, Ukraine, and Laboratoire Francis Perrin (URA CEA CNRS 2453), IRAMIS/Service des Photons, Atomes et Molécules, CEA Saclay, Bât. 522, 91191 Gif-sur-Yvette Cedex, France

Received: December 2, 2008; Revised Manuscript Received: February 9, 2009

A novel kinetic approach based on ab initio calculated rate constants has been developed and implemented in the kTSim program. The proposed approach allows prediction of the distribution of reactant and product concentrations over time, based exclusively on computationally obtained rate constants. The newly developed methodology was used to simulate the process of evaporation and tautomerization of guanine and cytosine under thermal ($T = 490$ K, cytosine; $T = 620$ K, guanine) and laser ($T = 1000$ K, 24 ns laser pulse) desorption conditions. Both monomolecular and bimolecular mechanisms of the tautomerization were considered simultaneously. The rates of the reactions were estimated using the values of Gibbs free energies calculated at the MPWB1K/aug-cc-pVDZ level and specified in a kTSim input. We expect that the proposed approach can also be used for accurate kinetic simulation of a wide range of processes.

I. Introduction

Nucleic acid bases cytosine and guanine represent DNA and RNA building blocks. These nucleobases together with adenine, thymine, and uracil are responsible for storage and transduction of genetic information.[1,2] Being incorporated into DNA, the nucleobases exist in one predominant keto form: CK for cytosine (Figure 1) and G9K for guanine (Figure 2). However, other "rare" tautomeric enol and imino forms are also known (Figures 1 and 2). These rare tautomers of the nucleobases have been suggested as a possible reason for spontaneous point mutations in DNA.[2−4] A recent investigation of the human genome has also revealed a number of single-nucleotide substitutions (point mutations) in the genome. This phenomenon is called "a single-nucleotide polymorphism" (SNP).[5] These substitutions are viewed as very sensitive biological markers for prediction of a specific individual response to certain drugs, susceptibility to environmental factors, and risk of disease development.[5,6]

Numerous computational data confirm an ability of cytosine and guanine to form rare tautomers in the gas phase.[4,9,10,17−26] Recently, remarkable progress in the understanding of photoexcitation and deactivation pathways of excited nucleobases has been achieved.[27−30]

Tautomers of nucleic acid bases could cause spontaneous point mutations with rates of $10^{-8}-10^{-10}$ (in vivo) and $10^{-6}-10^{-5}$ (in vitro).[7,8] In other words, their concentrations are extremely small and can hardly be detected even with modern experimental techniques. In addition, due to small concentrations the enol and imino tautomers have not been observed in the condensed phase. However, experiments performed in the gas phase indicate the presence of rare tautomers. Therefore, experimental techniques such as matrix isolation,[9] the He nanodroplet method,[10,11] and resonance-enhanced multiphoton ionization (REMPI) spectroscopy[12−16] are the main sources of experimental information on the physical and chemical properties of canonic and rare tautomers. However, each of the techniques requires very different conditions. In the matrix isolation and He nanodroplet experiments thermal desorption is used for sample evaporation, while in the REMPI experiments laser desorption is employed.

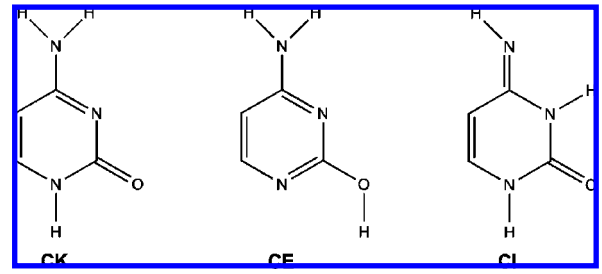

Figure 1. Cytosine canonic keto (CK) and rare enol (CE) and imino (CI) tautomers.

Thus, the experimental results sometimes differ in the structure and concentration of the observed tautomers. Furthermore, REMPI spectroscopy is limited in its ability to measure the concentrations of the observed tautomers.

To overcome these restrictions of the experimental techniques, here we have modeled evaporation of a solid sample of selected DNA bases and estimated the relative populations of the tautomers. Ab initio methods were employed to predict the

* To whom correspondence should be addressed. Phone: (601) 979-3723. Fax: (601) 979-7823. E-mail: jerzy@ccmsi.us.
[†] Jackson State University.
[‡] Institute of Molecular Biology and Genetics, National Academy of Sciences of Ukraine.
[§] STC "Institute for Single Crystals", National Academy of Sciences of Ukraine.
[∥] CEA Saclay.

10.1021/jp810570w CCC: $40.75
Published on Web 04/07/2009

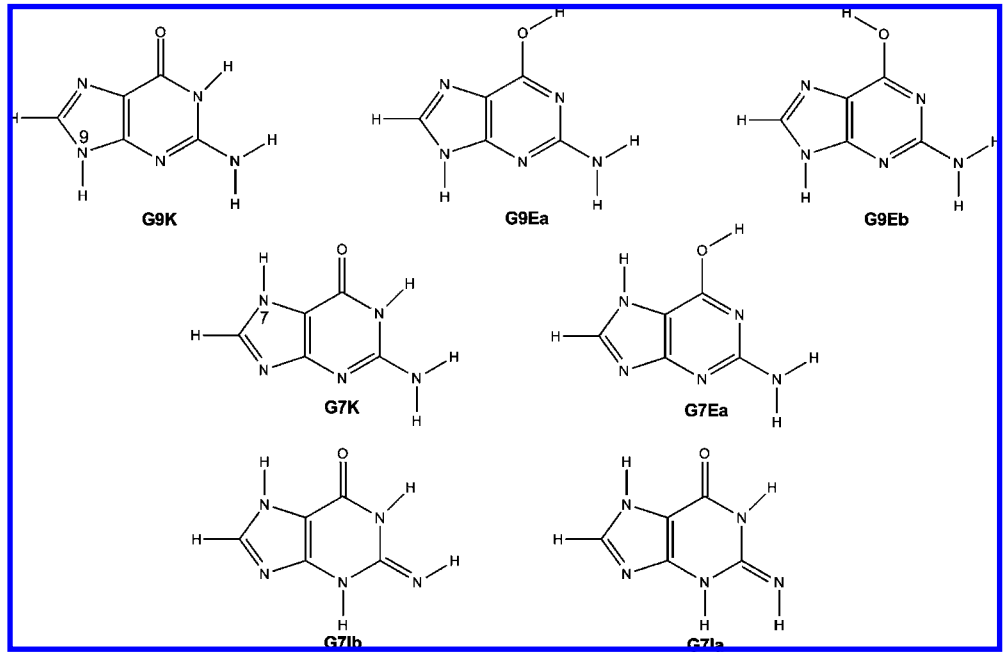

Figure 2. Guanine keto (G9K, G7K), enol (G9Ea, G9Eb, G7Ea), and imino (G7Ia, G7Ib) tautomers.

thermodynamic and kinetic parameters of the tautomerization processes. The only empirical value used in the present study is the nucleobase evaporation rate.

The solid sample of cytosine (guanine) consists only of the keto form, while a gas-phase mixture contains *keto* and rare tautomers. Thus, the vaporization kinetics accompanied by tautomeric transitions should be considered.

Similarly to our previous works,[17,18,22] this study is fully based on the ab initio calculated thermodynamic and kinetic parameters. Therefore, the presented model does not require any experimental rate constants. Moreover, the current approach can be used for investigation of the kinetics of fast reactions that is difficult (or impossible) to observe experimentally.

The paper is organized as follows. The Methodology section describes the kinetic model of thermal and laser desorption: kinetic equations, implementation of the model, and details of the ab initio quantum chemical calculations. The ab initio obtained thermodynamic and kinetic parameters of the tautomerization process are presented in the Results and Discussion section. Pathways of cytosine and guanine tautomerization are also discussed in this section. The conclusions on the mechanisms of nucleobase tautomerization in REMPI and matrix isolation experiments as well as the composition of the final gas-phase mixture are described in the last section.

II. Methodology

The study is focused on the low-energy tautomers observed experimentally (Figures 1 and 2). Let us start the consideration of guanine and cytosine tautomerization from construction of a general kinetic model of the processes. To estimate relative populations of the tautomers, two processes should be taken into account: evaporation of a solid sample and tautomerization on the surface (or in the gas phase) during the experimental desorption stage. The temperature and duration of the processes depend on the evaporation technique used in the experiment. Since thermal and laser desorption are commonly used in the gas-phase experiments, these two techniques are considered below.

II.1. Kinetic Model of Thermal Desorption. Thermal desorption is the common step for most matrix isolation experiments,[9] including isolation in He nanodroplets.[10,11] A solid sample of cytosine (guanine) is thermally evaporated in a furnace at a constant temperature of 490 K[9,10] (620 K).[11]

Due to the similarity of the kinetic equations describing tautomerization of cytosine and guanine, a general formalism disregarding the nature of the nucleobase will be introduced first.

According to the experimental data,[9,10] the gas-phase concentrations of canonic and rare forms of cytosine and guanine correspond to the Boltzmann equilibrium distribution at the temperature of the furnace. In equilibrium at temperatures of 490 K (cytosine) and 620 K (guanine), crystal samples are fully evaporated. Therefore, in our model it was assumed that under thermal desorption conditions all tautomeric transitions occur in the gas phase.

Another experimental observation[10] suggests that cytosine monomers and dimers have concentrations of the same order of magnitude, and no intermolecular complexes larger than dimers have been observed.[10] It was assumed in our model that all tautomeric transitions take place exclusively in monomers and dimers and the effect of larger clusters could be neglected.

On the basis of these assumptions, the kinetic model of thermal desorption of DNA bases should include the following steps: (i) formation of a dimer (D) from nucleobases M_1 and M_2; (ii) tautomerization of two monomers via the bimolecular mechanism with formation of the tautomeric dimer (D*); (iii) dimer decomposition with formation of two tautomers (M_1* and M_2*). The following tautomerization scheme can finally be drawn:

$$M_1 + M_2 \overset{K_D}{\rightleftharpoons} D \underset{k_D^{-1}}{\overset{k_D}{\rightleftharpoons}} D^* \overset{K_{D^*}}{\rightleftharpoons} M_1^* + M_2^* \qquad (1)$$

The monomolecular mechanism of transformation for each canonic form (M_i) to tautomer (M_i*) was also taken into account using a simple scheme:

$$M_i \underset{k_M^{-1}}{\overset{k_M}{\rightleftarrows}} M_i^* \qquad (2)$$

The population of the dimers depends on the vapor pressure, which controls the probability of collisions between monomers to form dimers.[10] In the present study it was assumed that dimers are present in abundance at thermal equilibrium, which is considered as the ideal condition for bimolecular tautomerization.[10] This equilibrium determines the relative concentrations of canonic (D) and tautomeric (D*) dimers:

$$K_{\mathrm{D}} = \frac{[\mathrm{D}]}{[\mathrm{M}_1][\mathrm{M}_2]},\ K_{\mathrm{D}^*} = \frac{[\mathrm{D}^*]}{[\mathrm{M}_1^*][\mathrm{M}_2^*]} \tag{3}$$

where K_{D} and K_{D^*} are the equilibrium constants for canonic and tautomeric dimers, respectively. The entire kinetic scheme consists of equations describing monomolecular tautomerization

$$\frac{\mathrm{d}[\mathrm{M}_i]}{\mathrm{d}t} = [\mathrm{M}_i^*]k_{\mathrm{M}}{}^{-1} - [\mathrm{M}_i]k_{\mathrm{M}}$$
$$\frac{\mathrm{d}[\mathrm{M}_i^*]}{\mathrm{d}t} = [\mathrm{M}_i]k_{\mathrm{M}}^{-1} - [\mathrm{M}_i^*]k_{\mathrm{M}} \tag{4}$$

and bimolecular tautomerization

$$\frac{\mathrm{d}[\mathrm{D}]}{\mathrm{d}t} = [\mathrm{D}^*]k_{\mathrm{D}}{}^{-1} - [\mathrm{D}]k_{\mathrm{D}}$$
$$\frac{\mathrm{d}[\mathrm{D}^*]}{\mathrm{d}t} = [\mathrm{D}]k_{\mathrm{D}}{}^{-1} - [\mathrm{D}^*]k_{\mathrm{D}} \tag{5}$$

The systems of kinetic equations (eqs 4 and 5) are coupled through equilibrium relations for dimers (eq 3).

II.2. Kinetic Model of Laser Desorption. Laser desorption represents the evaporation technique widely used in REMPI experiments.[14,15] Laser-induced desorption is a fast process in comparison to thermal desorption. According to the laser desorption scheme, evaporation of the solid nucleobase sample is controlled by several parameters: the temperature, pulse duration, and wavelength. The temperature during desorption rapidly rises from 300 to 1100 K with a $10^{10}-10^{11}$ K/s rate[31,32] and then decreases due to multiple intermolecular collisions. The gas-phase mixture after evaporation is cooled by jet expansion of carrier gas to a temperature of a few tens of kelvin.[14] Thus, it was assumed in our model that all tautomeric transitions take place in proximity of the solid surface where the temperature is high enough to promote tautomerization. The absence of tautomeric transitions in the gas phase at a temperature of 30 K is confirmed in section III.2.2.

A temperature profile has not been included directly in our model. The temperature change was modeled by setting the initial temperature to 1000 K followed by cooling due to sample transfer to the gas phase with evaporation rate constant k_{ev}. The rate constant of solid sample evaporation k_{ev} depends on the laser pulse parameters and intermolecular interactions on the solid sample surface. It was experimentally determined that the evaporation rate constant is comparable with the rate of temperature change.[14,30,31] To make the model simpler and decrease the number of parameters, the effective rate constant for evaporation was estimated on the basis of the duration of the temperature pulse in Hall's simulations.[31] The evaporation rate constant k_{ev} with assumption of constant laser pulse energy is related to the pulse duration τ as follows: $k_{\mathrm{ev}} = 1/\tau$. The estimated evaporation rate constant for a $\tau = 24$ ns pulse is $k_{\mathrm{ev}} = (24 \times 10^{-9})^{-1}\ \mathrm{s}^{-1} = 4.17 \times 10^{7}\ \mathrm{s}^{-1}$. It was also assumed that evaporation of all tautomers in monomolecular and dimer forms proceeds with the same rate constant k_{ev}. Thus, the evaporation rate constant k_{ev} is the only empirical parameter in our model. This simple scheme allows one to simulate different conditions and samples.

Finally, the kinetic equations describing laser-induced desorption of the tautomer in both monomer and dimer forms can be written as

$$\frac{\mathrm{d}[\mathrm{L}^{\mathrm{gas}}]}{\mathrm{d}t} = k_{\mathrm{ev}}[\mathrm{L}^{\mathrm{solid}}]$$
$$\frac{\mathrm{d}[\mathrm{L}^{\mathrm{solid}}]}{\mathrm{d}t} = -k_{\mathrm{ev}}[\mathrm{L}^{\mathrm{solid}}] \tag{6}$$
$$\mathrm{L} \in \{\mathrm{M}_i, \mathrm{D}, \mathrm{M}_i^*, \mathrm{D}^*\}$$

where $[\mathrm{L}^{\mathrm{solid}}]$ denotes the population in the solid phase (on the surface) of canonic and rare tautomers in both monomolecular and dimer forms, $[\mathrm{L}^{\mathrm{gas}}]$ represents the corresponding population after evaporation in the gas phase, and k_{ev} is the rate constant of evaporation.

The description of the tautomeric transitions in laser desorption experiments is similar to that in thermal desorption except the temperature change discussed above.

It should also be emphasized that no electronic excitations in nucleobases take place during laser desorption. Nd:YAG laser radiation (1064 nm) used for desorption is absorbed by the graphite where solid nucleobases are deposited. However, nucleobases do not absorb at this wavelength.[14,15] Thus, laser radiation energy is transferred to the nucleobases only in the form of heat and does not lead to electronic excitations in the nucleobases.

To describe tautomerization and evaporation of nucleobases in laser desorption experiments, eqs 4 and 5 have to be combined with eq 6.

Finally, one should note that the equilibrium constants of the dimer formation (eq 3) depend on the temperature. The rate constants k_{M}, $k_{\mathrm{M}}{}^{-1}$, k_{D}, and $k_{\mathrm{D}}{}^{-1}$ in eqs 4−6 also depend on the temperature. Details of the rate and equilibrium constant calculations are discussed in the next section.

II.3. Ab Initio Calculations. The relative Gibbs free energies for potential energy minima and transition states of the nucleobase monomers and dimers were calculated by applying the hybrid meta density functional MPWB1K[33] using augmented by diffuse functions Dunning's double-ζ correlation-consistent basis set,[34] aug-cc-pVDZ. This functional has been suggested for estimation of thermodynamic and kinetic parameters.[33] All quantum chemical calculations were performed using the Gaussian03[35] package.

To complete the kinetic model and solve kinetic equations, the equilibrium constants K_{D} and K_{D^*} in eq 3 and rate constants k_{D}, k_{M}, $k_{\mathrm{D}}{}^{-1}$, and $k_{\mathrm{M}}{}^{-1}$ in eqs 4 and 5 should be estimated.

The equilibrium constants were calculated using the standard equation $K = \exp(-\Delta G/RT)$, where ΔG is the relative total Gibbs free energy of the reactant and product, T is the temperature, and R is the universal gas constant. Standard transitional state theory[37] was employed to estimate the rate constants as follows:

$$k = \frac{k_{\mathrm{b}}T}{h}\exp\left(-\frac{\Delta G^{\ddagger}}{RT}\right) \tag{7}$$

where $\Delta G^{\ddagger}$ is the activation Gibbs free energy of the reaction, T is the temperature, k_{b} is Boltzmann's constant, h is Plank's constant, and R is the universal gas constant.

TABLE 1: Calculated and Experimental Relative Gibbs Free Energies (Δ*G*, kcal/mol) and Boltzmann Populations (Pop, %) of the Three Experimentally Observed Cytosine Tautomers

	MPWB1K[a]		MP2[b]		CCSD(T)[c]		matrix[d]		
	Δ*G*	Pop	Δ*G*	Pop	Δ*G*	Pop	Pop	drop[e,g]	REMPI[f,g]
CK	0.28	42.37	1.41	26.35	1.46	26.46	26.67−28.57	+	+
CE	0.00	56.50	0.00	67.57	0.00	44.84	66.67−57.14	+	+
CI	4.03	1.13	3.17	6.08	1.79	28.70	6.67−14.29	−	−

[a] MPWB1K/aug-cc-pVDZ//MPWB1K//aug-cc-pVDZ, $T = 490$ K. [b] Reference 26, MP2(full)/6-311+G(2d,2p)//MP2(full)/6-31G(d), $T = 490$ K. [c] Reference 46, CCSD(T)/cc-pVTZ//CCSD/TZP, MP2/TZP (vibrational frequencies at MP2/TZP), $T = 470$ K. [d] Reference 9, matrix isolation, $T = 493$ K. [e] Reference 10, He nanodroplets, $T = 483$ K. [f] Reference 12. [g] Assignment of the tautomers observed.

TABLE 2: Calculated and Experimental Relative Electronic Energies (Δ*E*, kcal/mol) or Gibbs Free Energies (Δ*G*, kcal/mol) and Boltzmann Populations (Pop, %) of the Guanine Tautomers

	MPWB1K[a]		MP2[b]		MP2(∞)[c]		CCSD(T)[d]		drop[e]			
	Δ*G*	Pop	Δ*E*	Pop	Δ*E*	Pop	Δ*E*	Pop	Pop	REMPI1[f,i]	REMPI2[g,i]	REMPI3[h,i]
G9K	0.40	20.51	0.72	23.53	0.72	22.07	0.77	24.26	31.80	+	+	−
G9Ea	0.13	25.64	1.05	18.07	0.90	19.07	1.64	11.97	14.64	+	−	−
G9Eb	0.31	22.22	1.29	14.71	1.02	17.30	1.27	16.17	11.72	−	+	+
G7K	0.00	28.49	0.00	42.02	0.00	39.59	0.0	45.33	41.84	+	+	−
G7Ea	3.02	2.56	3.85	1.68	3.70	1.97	3.69	2.27	31.80	−	+	+
G7Ia	6.28	0.28								−	−	+
G7Ib	6.19	0.28								−	−	+

[a] MPWB1K/aug-cc-pVDZ//MPWB1K//aug-cc-pVDZ, $T = 620$ K. [b] Reference 26, MP2(full)/6-311+G(2d,2p)//MP2(full)/6-31G(d), $T = 490$ K. [c] Reference 18, MP2 extrapolated to infinite basis set. [d] Referecne 21, CCSD(T)/aug-cc-pVDZ//MP2/aug-cc-pVDZ. [e] Reference 11, He nanodroplets, $T = 623$ K. [f] Reference 14. [g] Reference 15. [h] Reference 16. [i] Assignment of the tautomers observed.

It should be noted that in the rate constant calculations the tunneling effect was neglected due to its minor contribution at the considered temperatures $T > 490$ K.[47]

II.4. Kinetic Model Implementation with the kTSim Program. The Kinetic Simulation (kTSim) program[36] has been developed to implement the considered formalism. The ab initio calculated equilibrium and rate constants and the experimentally estimated desorption rate values were specified in kTSim input. In the present work the kTSim program was used to estimate the population of cytosine and guanine in gas-phase experiments under thermal and laser desorption conditions.

The concentrations of the tautomers on the subsequent step $\mathbf{n}(t + \Delta t)$ of the simulation were calculated using the concentrations from the previous step $\mathbf{n}(t)$:

$$\mathbf{n}(t + \Delta t) = \mathbf{F}(\mathbf{n}(t))$$

where $\mathbf{n}(t)$ is the vector of the concentrations at the considered moment of time t, Δt is the time step of the integration, and $\mathbf{F}$ is the operator which performs propagation of the concentrations over time. The operator $\mathbf{F}$ is represented by eqs 4−6. Evaluation of the operator $\mathbf{F}$ scales as $\sim N^2/2$, where N is the number of considered tautomers. The rate constant matrix has dimensions $N \times N$ and describes all pair transitions between the tautomers. Since the rate constant matrix is sparse and the number of pair transitions (nonzero elements of the matrix) is less than $N^2/2$, evaluation of $\mathbf{F}$ can be improved. The nonzero elements of the rate constant matrix can be rearranged in a one-dimensional array of size m ($m < N^2/2$). Then evaluation of the operator $\mathbf{F}$ requires evaluation of the one-dimensional array and scales linearly as $\sim m$, where m is proportional to the number of reactions (tautomeric transitions) considered in the system.

Integration of the system was performed using the fourth-order Runge−Kutta method.[38−40] The accuracy of the calculations was checked using the fifth-order Dormand−Prince method[38,41] and the normalization conditions. The results of the simulations are presented in the next section.

III. Results and Discussion

III.1. Evaluation of the MPWB1K Functional. To evaluate the accuracy of the simulation of the tautomerization processes initiated by thermally induced or laser-induced evaporation, the accuracy of the selected computational method (DFT/MPWB1K) should be checked. This verification could be done by the comparison of the results with available experimental and other ab initio data obtained at high levels of theory. Those data are available for the relative populations of cytosine tautomers at $T = 490$ K and guanine tautomers at $T = 610$ K in the gas phase and are presented in Tables 1 and 2.

All the considered methods reveal the same tautomer (CE for cytosine and G7K for guanine; see Figures 1 and 2) as the most thermodynamically stable. Also, they predict similar populations of the equilibrium mixture (CE, CK, and CI for cytosine; G7K, G9K, G9Ea, and G9Eb for guanine). The calculated results for cytosine are in good agreement with the experimental values, while comparison of the results for guanine is hindered due to discrepancy between available experimental results. The presented data (Tables 1 and 2) suggest that the MPWB1K functional works with approximately the same accuracy as much more resource demanding MP2 and CCSD(T) approximations.

There are no data on the rates of tautomeric transitions in gas-phase experiments. Thus, we cannot directly test the accuracy of the calculated activation energies and rate constants of reactions. According to Zhao and Truhlar,[33] the MPWB1K functional was specially designed to simulate thermochemistry and kinetics experiments. The accuracy of MPWB1K in the activation barrier data is similar to that of the calculations at the QCISD(T) level (MUE(MPWB1K) = 1.29 kcal/mol, MUE(QSISD(T)) = 1.24 kcal/mol).[48]

III.2. Cytosine. ***III.2.1. Kinetics of Thermal Desorption.*** The cytosine crystal[42] consists of CKKb dimers formed by canonic CK tautomers (Figures 1 and 3) bound by H bonds. Therefore, on the basis of the experimental results,[10,14,42] we

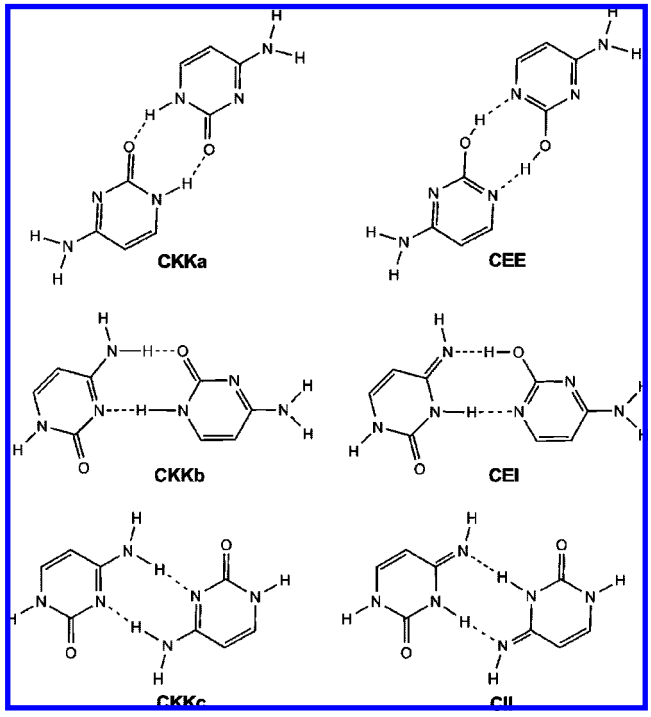

Figure 3. Tautomerization in cytosine dimers. CKKa produces only enol tautomers (CEE), CKKb produces both enol and imino tautomers (CEI), and CKKc produces only imino tautomers (CII).

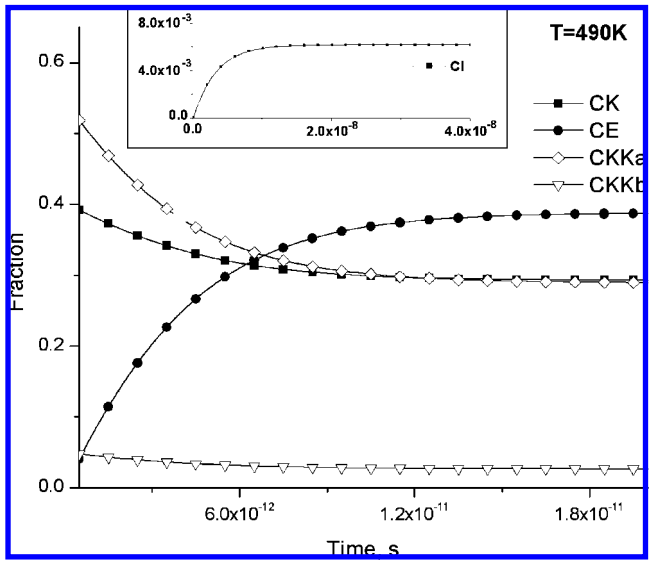

Figure 4. Kinetics of cytosine tautomerization induced by thermal desorption at 490 K

expect that cytosine desorbs from the crystal surface in the form of CK monomers and dimers.

According to eqs 1 and 2, the following interactions and tautomeric transitions should be taken into account in our modeling:

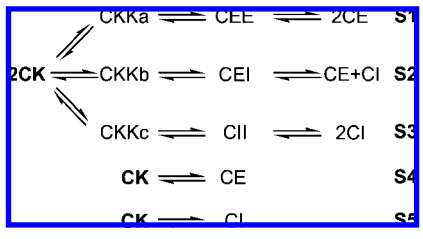

TABLE 3: Relative Gibbs Free Energies (ΔG, kcal/mol) and Equilibrium Constants of Tautomerization (K_{eq}) of Cytosine Tautomers and Their Dimers Formed Under Thermal (T = 490 K) and Laser (T = 1000 K) Desorption Conditions, Calculated at the MPWB1K/aug-cc-pVDZ Level

	490 K		1000 K	
	ΔG	K_{eq}	ΔG	K_{eq}
CK ⇄ CE	−2.06	1.327	0.74	6.901×10^{-1}
CK ⇄ CI	3.75	2.121×10^{-2}	5.48	6.340×10^{-2}
2CK ⇄ CKKa	−1.19	3.38	17.39	1.59×10^{-4}
2CK ⇄ CKKb	1.14	3.11×10^{-1}	20.98	2.61×10^{-5}
2CK ⇄ CKKc	4.79	7.34×10^{-3}	25.73	2.38×10^{-6}
CEE ⇄ 2CE	3.75	2.13×10^{-2}	21.86	1.67×10^{-5}
CEI ⇄ CE + CI	5.10	5.31×10^{-3}	24.12	5.35×10^{-6}
CII ⇄ 2CI	5.72	2.82×10^{-3}	23.50	7.33×10^{-6}

The chemical structures of all species involved in the above scheme are presented in Figures 1 and 3. The thermodynamic and kinetic parameters which characterize the processes presented in the scheme (reactions S1−S5) are collected in Tables 3 and 4.

Pathways S4 and S1 are accompanied by a negative ΔG value. Thus, they are the most thermodynamically favorable channels for the CK transformation. Since the barrier of tautomerization in dimers (e.g., S1) is ca. 20 kcal/mol lower than in monomers (e.g., S4) (see Table 4), the reaction rate of monomeric tautomerization is much lower if compared to that of tautomerization in dimers. This means that the rate of tautomerization via the bimolecular mechanism is 10^{10} faster than via the monomolecular one. Thus, bimolecular processes might have major contributions to the tautomerization of the nucleobases.

Kinetic eqs 3−5 were applied to the reactions S1−S5. The results are presented in Figure 4. Initial concentrations of CK, CKKa, CKKb, and CKKc correspond to the thermodynamic equilibrium at 490 K: 40.2% (CK), 54.6% (CKKa), 5% (CKKb), and 0.1% (CKKc). The corresponding equilibrium constants are presented in Table 3.

The obtained results confirm that the decay of CK via a CKKa dimer is the main channel for CE formation. Despite CK involvement in several interactions and transformations, the comparison of the relative Gibbs free energies and rate constants responsible for inter- and intramolecular tautomerization suggests that the S1 channel dominates over the others (S2−S5).

It has been shown that the major fraction of tautomers (CK, CE, CKKa, CEEb) reaches equilibrium within 2×10^{-11} s. However, formation of CI tautomers requires ca. 4×10^{-8} s. This suggests that CI formation proceeds via the bimolecular mechanism through formation of CKKb (Table 4).

The composition of the cytosine tautomeric mixture is given in Table 5. Our simulation suggests that a significant amount (ca. 30%) of cytosine dimers is present in the tautomeric mixture. This fact is in qualitative agreement with experiments by Miller et al.,[10] who observed a certain amount of dimers. As expected, the composition of the mixture of cytosine tautomers at 490 K after 4×10^{-8} s predicted at the MPWB1K level virtually reproduces the equilibrium concentrations of isolated CK, CE, and CI tautomers.

III.2.2. Kinetics of Laser-Induced Desorption. Similarly to the considered thermal desorption, the set of chemical equilibria and tautomeric transitions (pathways S1−S5) was considered. The corresponding thermodynamic and kinetic parameters are collected in Tables 3 and 4. As expected, due to an increase of temperature to 1000 K, the relative Gibbs free energies of dimer formation are much higher; in particular, there are no negative

TABLE 4: Activation Gibbs Free Energies ($\Delta G^{\ddagger}$, kcal/mol) and Rate Constants of Forward (k_f, s^{-1}) and Reverse (k_r, s^{-1}) Tautomerization Reactions in Monomers and Dimers of Cytosine Under Thermal ($T = 490$ K) and Laser ($T = 1000$ K) Desorption Conditions, Calculated at the MPWB1K/aug-cc-pVDZ Level

	490 K			1000 K		
	$\Delta G_f^{\ddagger}$	k_f	k_r	$\Delta G_f^{\ddagger}$	k_f	k_r
CK ⇄ CE	34.14	6.06×10^{-3}	4.56×10^{-3}	35.72	3.25×10^{5}	4.71×10^{5}
CK ⇄ CI	41.88	2.15×10^{-6}	1.01×10^{-4}	44.13	4.72×10^{3}	7.44×10^{4}
CKKa ⇄ CEE	4.08	1.54×10^{11}	1.39×10^{13}	4.81	1.85×10^{12}	3.69×10^{13}
CKKb ⇄ CEI	10.39	2.37×10^{-8}	4.92×10^{11}	13.89	1.92×10^{10}	2.14×10^{12}
CKKc ⇄ CII	13.99	5.91×10^{6}	3.42×10^{10}	17.11	3.80×10^{9}	3.08×10^{11}

TABLE 5: Composition (%) of the Cytosine Gas-Phase Mixture under Thermal (in 4×10^{-8} s) and Laser (in 1×10^{-7} s) Desorption Conditions

	4×10^{-8} s[a]	1×10^{-7} s[b]
CK	29.11 (41.0)[c]	60.40 (57.0)[d]
CE	38.63 (54.4)[c]	37.92 (39.3)[d]
CI	0.62 (0.9)[c]	0.13 (3.6)[d]
CKKa	28.63	3.2×10^{-3}
CKKb	2.63	5.32×10^{-4}
rest[e]	0.38	4.87×10^{-5}

[a] At 490 K. [b] At 1000 K. [c] The composition takes into account only the population of CK, CE, and CI tautomers. [d] Equilibrium concentration at 1000 K. [e] Total concentrations of CKKc, CEE, CEI, and CII.

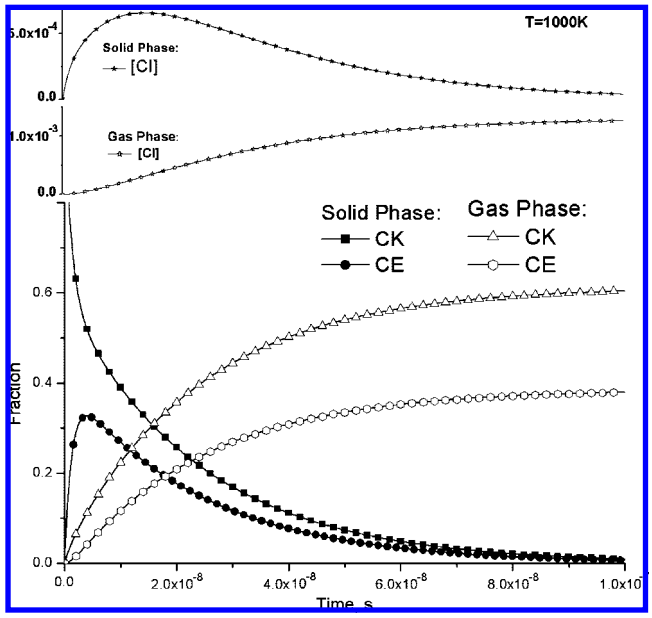

Figure 5. Kinetics of cytosine tautomerization induced by laser desorption.

values observed. Therefore, all equilibria are significantly shifted to the direction of CK tautomer formation.

Initial concentrations were chosen similarly to those described in the previous section, and the initial mixture consisted of CK (99.98%), CKKa (1.6×10^{-2}%), CKKb (2.6×10^{-3}%), and CKKc (2.4×10^{-4}%).

The application of eqs 4−6 to pathways S1−S5 provides more complex behavior of the kinetic curves than observed under thermal desorption conditions. As follows from Figure 5, the desorption process consists of two stages: (i) fast tautomerization on the solid-phase surface via the bimolecular mechanism; (ii) evaporation of all cytosine forms (CK, CE, CI, CKKa, CKKb, CKKc) with domination of CK and CE.

The first tautomerization stage takes approximately 10^{-9} s and is characterized by fast depletion of the CK form and a fast increase of CE on the solid surface due to very fast tautomerization through the bimolecular mechanism with a rate constant of 10^{11} s^{-1}. Similarly to thermal desorption, mechanism S1 is the most favorable.

At the second stage after a 2×10^{-8} s period, desorption of the tautomers dominates and the mixture of tautomers starts to evaporate into the gas phase. The concentration of the CK and CE forms is the highest, and the process of desorption ends within 1×10^{-7} s, according to the rate of desorption. One might see that all equilibria except CK ↔ CE are characterized by quite high values of relative Gibbs free energies (Table 3). This means that all considered equilibria except CK ↔ CE are strongly shifted to the left side of the chemical equations. This is a plausible reason for the absence of the imino form in REMPI spectra of cytosine.[12,13] Also dimers are almost absent in the mixture (Table 5). Nevertheless, when the temperature drops to a few tens of kelvin in the gas phase, the dimers can be regenerated. However, no dimers were recorded in the gas-phase experiments, because of the mass selectivity of REMPI experiments. In our model no tautomeric transitions in the gas phase were considered due to the low temperature and pressure in the gas phase.

Analysis of populations of tautomers in the gas phase (Table 5) and comparison with the corresponding equilibrium values (Table 3) shows that distribution of the tautomers is close to that in equilibrium at 1000 K.

In the case of laser desorption it was assumed in our model that the tautomeric mixture is formed in proximity of the solid sample surface at a temperature 1000 K. Since the mixture is cooled to a few tens of kelvin, the tautomerization rate at 30 K was estimated. Considering a minimal barrier of tautomerization of 4.5 kcal/mol (Table 4), the corresponding rate constant of tautomerization was estimated as 6.744×10^{-24} s^{-1} at 30 K. Then the estimated time for the rare tautomer to reach a population of at least 0.01% is ca. 1.5×10^{20} s (many years). This time is absolutely incomparable with any reasonable registration time. Thus, one can conclude that at a temperature of a few tens of kelvin tautomeric transitions cannot proceed due to the extremely low tautomerization rate.

III.3. Guanine. ***III.3.1. Kinetics of Thermal Desorption.*** The structure of guanine monohydrate was reported in 1971 by Thewalt et al.[43] (Figure 6a). Only the G9K tautomer has been observed in the study.[43] The same G9K tautomer has also been found in nucleic acids and obviously considered as a canonic form. However, the recently investigated structure of anhydrous guanine reported in 2006 by Guille et al.[44] from the synchrotron X-ray diffraction experiment demonstrated exclusive presence of G7K (Figure 6b). Moreover, the results of ab initio calculations suggest that the G7K tautomer is the most stable in the gas phase.[18]

Analysis of the G9K and G7K structures revealed that there is no reasonable pathway found for tautomerization between G7K and G9K tautomers either in the gas phase or in crystal.

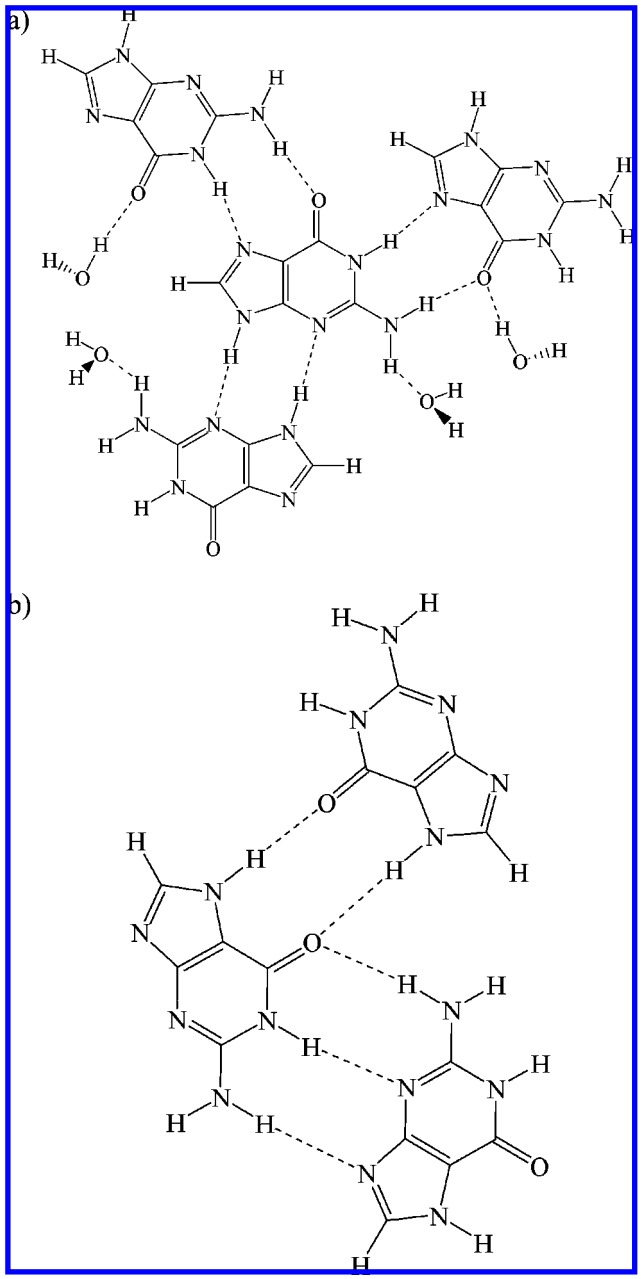

Figure 6. Guanine crystal structure viewed perpendicular to the sheet of molecules: (a) guanine monohydrate (only G9K observed);[43] (b) anhydrous guanine (only G7K observed).[44] The dashed lines represent hydrogen bonds.

Therefore, the only possibility for G9K and G7K presence is formation of these tautomers during the preparation process in solution.

Further analysis of guanine crystal structures revealed that dimers contributing to the guanine tautomerization via the bimolecular mechanism are not present in guanine monohydrate (Figure 6a). The structure of anhydrous guanine (Figure 6b) is more promising because it contains the G7K9K dimer, which could produce G7E and G7I tautomers reported by Mons et al.[16]

Since the exact structure of the sample containing both G9K and G7K tautomers is unknown, we consider all possible dimers which could produce tautomers via the bimolecular mechanism. The comprehensive study of guanine dimers has been done by Nir et al.[45] Among all possible guanine dimers studied, the four dimers G9K9K, G9K7Ka, G9K7Kb, and G7K7K displayed in Figure 7 are able to produce low-energy tautomers via the bimolecular mechanism and thus contribute to tautomerization of G9K and G7K. Two of the dimers (G9K7K7a and G9K7K7b) have been recorded experimentally.[45] The G7K7K is the only dimer present in anhydrous guanine.[44]

On the basis of the analysis of the crystallographic data[43,44] and investigation by Nir et al.,[45] similarly to cytosine, we expect the following interactions and tautomeric transitions are of importance:

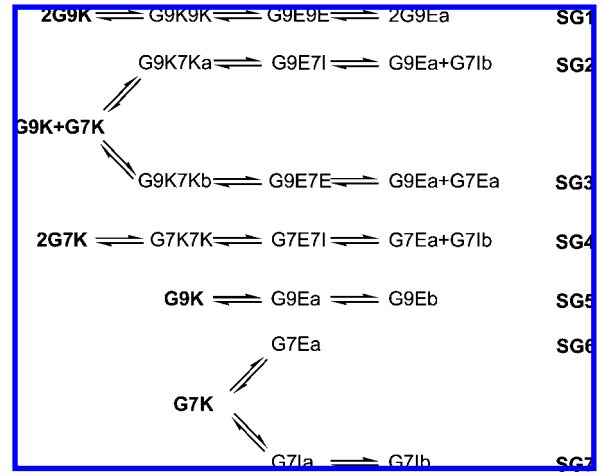

The corresponding chemical structures are depicted in Figures 2 and 7. The thermodynamic and kinetic parameters are collected in Tables 2, 6, and 7. Similarly to the case of cytosine, among all possible pathways of guanine tautomerization (SG1−SG7, Table 7), only a few of them result in a significant rate of G9K and G7K transformation into their enol and imino tautomers. Channels SG1−SG4 originating from the dimers are more preferable due to low activation barriers. In contrast, pathways SG5−SG7, which include intramolecular transitions, require much more energy for activation and therefore are slower.

Similarly to modeling of cytosine thermal desorption, initial concentrations of the guanine dimers (G9K9K, G9K7Ka, G9K7Kb, G7K7K) are determined by their relative Gibbs free energies of formation at 620 K (see Tables 2 and 6). Therefore, under the initial conditions the mixture composition was G9K (15.2%), G7K (52.4%), G9K9K (22.9%), G9K7Ka (1.1%), G9K7Kb (6.7%), and G7K7K (1.9%).

The detailed analysis of the kinetic curves (see Figures 8 and 9) shows that the processes consist of two stages. The faster stage corresponds to tautomerization via the SG1 and SG3 channels. In addition, monomolecular transitions in rotamers (channel SG5) are quite fast due to a low activation energy value (see Table 7). As expected from the analysis of equilibrium constants, the canonic dimer G9K9K dominates over the others. The second stage of guanine thermal tautomerization is relatively slower (Figure 9). It is completed within 5×10^{-6} s and includes the SG2 and SG4 pathways. The monomolecular SG7 channel responsible for the equilibration between the *syn* and *anti* rotamers of the imino forms also contributes to the whole process.

We have not found any kinetically reasonable channel which would be responsible for transformation between the G9 and G7 forms of guanine tautomers. In fact, there are two separate mixtures of tautomers which cannot be transformed into each other through reactions SG1−SG7. Therefore, we do not discuss whether the total system has reached the equilibrium composi-

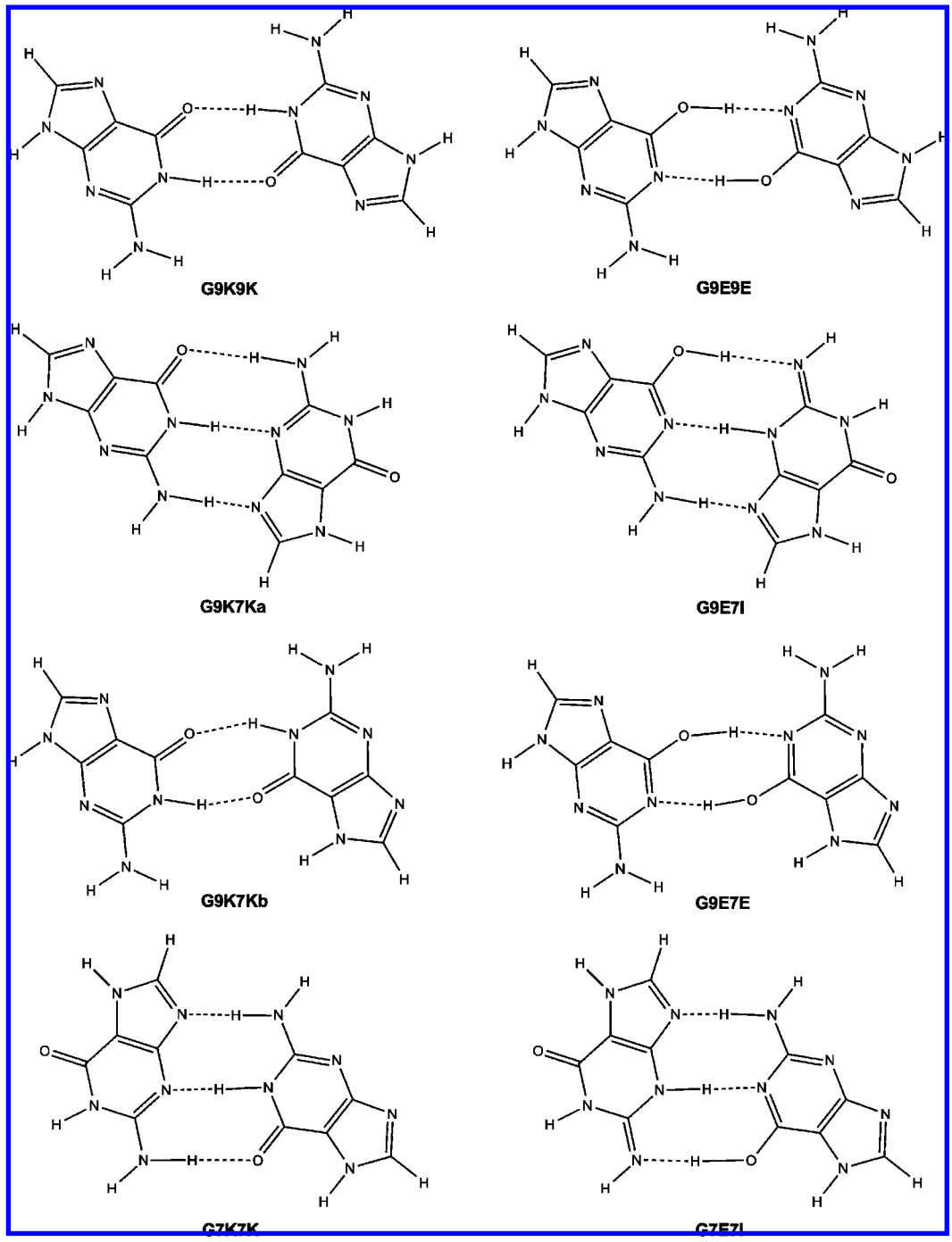

Figure 7. Considered guanine dimers.

tion. Instead, we have focused on prediction of whether the steady state for this tautomeric mixture is reached after ca. 5.0 $\times 10^{-6}$ s and results in the concentrations of guanine tautomers displayed in Table 8. In particular, the thermodynamically most stable G9K, G9Ea, G9Eb, and G7K tautomers have been observed in He nanodroplets.[11]

III.3.2. Kinetics of Laser-Induced Desorption. The initial distribution of guanine tautomers under laser desorption conditions was chosen similarly to that of thermal desorption but at an initial temperature of 1000 K. The initial mixture consisted of monomers G9K (41.68%) and G7K (58.09%) and dimers G9K9K (0.17%), G9K7Ka (7.19 $\times 10^{-3}$%), G9K7Kb (4.32%), and G7K7K (9.03%). Similarly to laser desorption of cytosine (section III.2.2), it was assumed that the tautomeric transitions take place only in proximity of the solid sample surface.

As follows from the graphs presented in Figure 10, guanine tautomerization under laser desorption conditions is more complex than the corresponding process for cytosine due to the larger number of intermediates and products. The SG1 pathway of tautomerization on the surface dominates over the others. Again, because of uncertainty with the channel of conversion between the G7 and G9 forms, we do not discuss the correspondence of the tautomeric mixture to the composition at thermodynamic equilibrium.

It was found that in spite of the high rate of laser desorption (4.17×10^{7} s^{-1}) bimolecular tautomerization ($10^{9}-10^{12}$ s^{-1}) is many orders faster than desorption. The present simulation results demonstrate the preference of the thermodynamically most stable keto and enol guanine forms in the gas-phase mixture. The absence of the three major components of the

TABLE 6: Relative Gibbs Free Energies (ΔG, kcal/mol) and Equilibrium Constants of Tautomerization (K_{eq}) of Guanine Tautomers and Their Dimers under Thermal (T = 620 K) and Laser (T = 1000 K) Desorption Conditions, Calculated at the MPWB1K/aug-cc-pVDZ Level

	620 K		1000 K	
	ΔG	K_{eq}	ΔG	K_{eq}
G9K ⇄ G9Ea	−0.27	1.247	−0.17	1.089
G9Ea ⇄ G9Eb	0.18	8.675×10^{-1}	0.03	9.841×10^{-1}
G7K ⇄ G7Ea	3.02	8.600×10^{-2}	2.88	2.342×10^{-1}
G7K ⇄ G7Ib	6.19	6.582×10^{-3}	6.10	4.656×10^{-2}
G7Ib ⇄ G7Ia	0.09	9.312×10^{-1}	0.06	9.710×10^{-1}
2G9K ⇄ G9K9K	−2.83	9.94	9.25	9.50×10^{-3}
G9K + G7K ⇄ G9K7Ka	2.50	1.32×10^{-1}	16.14	2.97×10^{-4}
G9K + G7K ⇄ G9K7Kb	0.24	8.25×10^{-1}	12.58	1.79×10^{-3}
G7K + G7K ⇄ G7K7K	3.27	7.03×10^{-2}	16.35	2.68×10^{-4}
G9E9E ⇄ G9Ea + G9Ea	6.59	4.76×10^{-3}	19.14	6.58×10^{-5}
G9E7I ⇄ G9Ea + G7Ib	7.44	2.39×10^{-3}	21.35	2.16×10^{-5}
G9E7E ⇄ G9Ea + G7Ea	7.34	2.59×10^{-3}	20.36	3.56×10^{-5}
G7E7I ⇄ G7Ea + G7Ib	6.98	3.48×10^{-3}	21.33	2.18×10^{-5}

TABLE 7: Activation Gibbs Free Energy ($\Delta G^{\ddagger}$, kcal/mol) and Rate Constants of Forward (k_f, s^{-1}) and Reverse (k_r, s^{-1}) Tautomerization Reactions in Monomers and Dimers of Guanine under Thermal (T = 620 K) and Laser (T = 1000 K) Desorption Conditions, Calculated at the MPWB1K/aug-cc-pVDZ Level

	620 K			1000 K		
	$\Delta G_f^{\ddagger}$	k_f	k_r	$\Delta G_f^{\ddagger}$	k_f	k_r
G9K ⇄ G9Ea	34.03	1.31×10^{1}	1.05×10^{1}	34.75	5.30×10^{5}	4.87×10^{5}
G9Ea ⇄ G9Eb	8.69	1.12×10^{10}	1.29×10^{10}	9.39	1.85×10^{11}	1.88×10^{11}
G7K ⇄ G7Ea	36.99	1.18	1.37×10^{1}	37.57	1.28×10^{5}	5.48×10^{5}
G7K ⇄ G7Ib	43.85	4.52×10^{-3}	6.87×10^{-1}	43.79	5.60×10^{3}	1.20×10^{5}
G7Ib ⇄ G7Ia	19.37	1.92×10^{6}	2.06×10^{6}	19.98	8.95×10^{8}	9.22×10^{8}
G9K9K ⇄ G9E9E	9.24	7.17×10^{9}	9.62×10^{12}	11.00	8.22×10^{10}	1.00×10^{13}
G9K7Ka ⇄ G9E7I	14.06	1.43×10^{8}	9.57×10^{11}	16.10	6.31×10^{9}	1.71×10^{12}
G9K7Kb ⇄ G9E7E	10.11	3.53×10^{9}	1.05×10^{13}	11.88	5.28×10^{10}	1.04×10^{13}
G7K7K ⇄ G7E7I	15.74	3.64×10^{7}	1.30×10^{12}	18.61	1.78×10^{9}	2.01×10^{12}

mixture (G9K, G7K, G9Ea) in the spectra[16] should be ascribed to the REMPI detection scheme itself. One of the reasons for the absence of the four most stable forms in the spectrum was seen in the intrinsic ultrafast radiationless $S_1 \rightarrow S_0$ transitions that prevent their observation.[16] Recent calculations[27,30] have also confirmed this assumption.

Thus, our simulation suggests that the tautomeric populations in the gas phase produced by thermal vaporization and laser desorption seem to be qualitatively similar, in the sense that the four most stable forms are the most abundant in both cases. The qualitative difference between thermal and laser desorption is essentially the lower abundance of the rare tautomers with laser desorption, i.e., those of relative energies higher than 3 kcal/mol, in disagreement with the intuitive idea that the higher temperatures of the laser desorption may favor the population

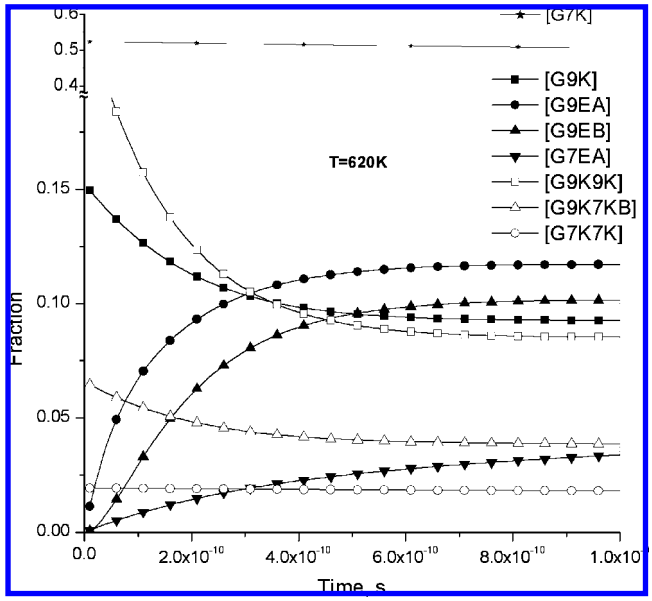

Figure 8. Kinetics of guanine tautomerization (fast step) induced by thermal desorption at 620 K. Only tautomers having a major contribution are shown.

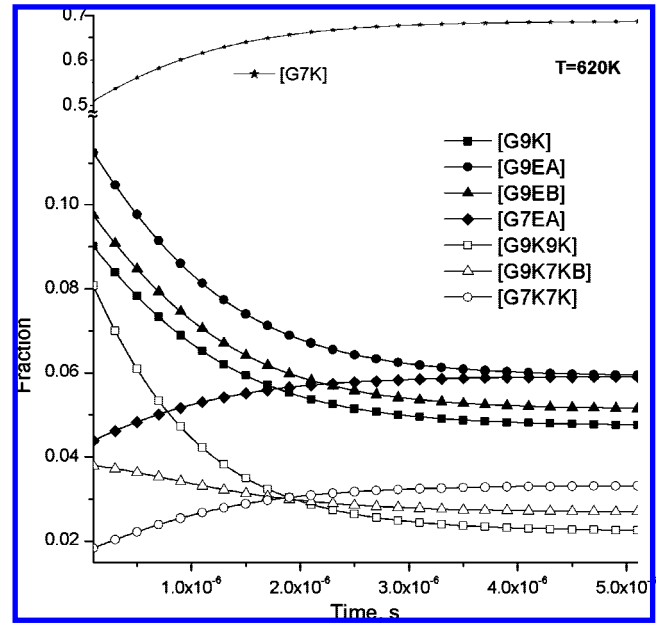

Figure 9. Kinetics of guanine tautomerization (slow step) induced by thermal desorption at 620 K. Only tautomers having a major contribution are shown.

TABLE 8: Composition (%) of the Guanine Gas-Phase Mixture under Thermally (in 1×10^{-5} s) and Laser (in 1×10^{-7} s) Induced Desorption

	1×10^{-5} s [a]	1×10^{-7} s [b]
G9K	4.74	15.94
G9Ea	5.91	13.10
G9Eb	5.13	12.89
G7K	68.75	53.29
G7Ea	5.91	4.55
G7Ia	0.42	0.10
G7Ib	0.45	0.10
G9K9K	2.23	0.02
G9K7Ka	0.43	1.50×10^{-3}
G9K7Kb	2.69	8.96×10^{-3}
G7K7K	3.32	3.95×10^{-3}
rest[c]	3×10^{-3}	6.65×10^{-5}

[a] At 620 K. [b] At 1000 K. [c] Total concentrations of G9E9E, G9E7I, G9E7E, and G7E7I.

of rare tautomers. These rare tautomers were not observed in the He nanodroplet experiment, in agreement with the low concentration predicted. On the contrary, the REMPI experiments carried out with laser desorption seem to lead to the following apparent paradox: The rare tautomers are the only species observed in spite of a very low relative concentration. This fact can be explained by the following combination of circumstances. As mentioned above, the REMPI experiments are practically blind to four of the most stable conformers.[16] The only signal observed is due to rare tautomers. It is expected to be weak because of the low concentration of these species. However, in the laser desorption experiments, the laser power is usually increased to values that provide an observable signal. Because of the high nonlinearity of the process, once the desorption threshold is reached, a relatively modest increase of this power leads to a huge increase of desorbed material, making relatively weak populations relatively large in terms of absolute values and therefore giving rise to detection of the rare tautomers. Comfortable absolute signals can even be achieved at the expense of the sample lifetime. Such a picture is in agreement with our experience that, with guanine, relatively high desorption powers have to be employed to obtain manageable signals,[32] resulting in short sample lifetimes and difficult experimental conditions (modest signal/noise ratios).

IV. Conclusions

In the present study a novel DFT-based kinetic approach for modeling gas-phase experiments was proposed. Mechanisms of cytosine and guanine tautomerization in gas-phase double-resonance and matrix isolation experiments with both thermal and laser desorption techniques were considered. The time dependence of the relative populations of tautomers during the desorption stage of the gas-phase experiments was estimated. The tautomerization of cytosine and guanine nucleobases under both thermal ($T = 490$ K, cytosine; $T = 620$ K, guanine) and laser ($T = 1000$ K, 24 ns laser pulse) desorption conditions was simulated. Both monomolecular and bimolecular mechanisms of tautomerization were taken into account. The rates of the reactions were estimated on the basis of the values of Gibbs free energies calculated at the MPWB1K/aug-cc-pVDZ level. The kinetic simulations suggest that the tautomerization in the nucleobases proceeds via the bimolecular mechanism. The concentrations of dimers under thermal and laser desorption conditions are very low. However, due to a very high rate of tautomerization the bimolecular mechanism dominates over the monomolecular one. The dimers are the major source of rare tautomers for cytosine and guanine. The concentration of the keto (canonic) and enol forms dominates. In laser desorption experiments the tautomerization proceeds in two steps: fast formation of tautomers on the surface and subsequent evaporation of the tautomers. In the case of the thermally induced and laser-induced gas-phase tautomerization of cytosine, the simulated data completely correspond to the results obtained experimentally and enhance experimental data by prediction that a laser-induced desorption of cytosine tautomers should proceed instantly to the equilibrium state at the temperature of desorption.

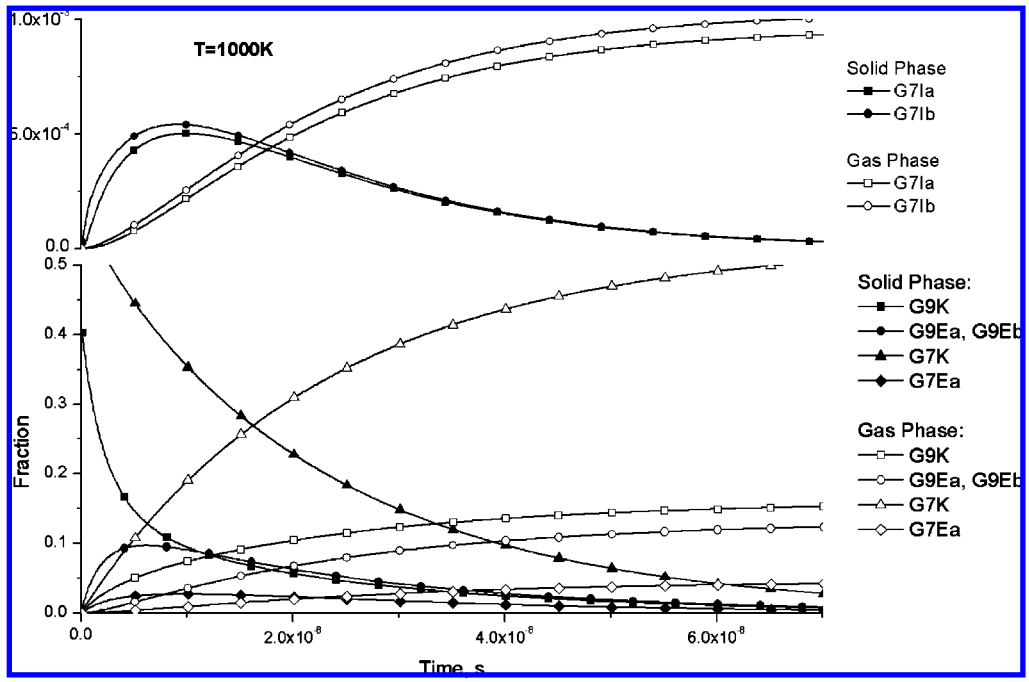

Figure 10. Kinetics of guanine tautomerization induced by laser desorption of the mixture at $T = 1000$ K. Only tautomers a having major contribution are shown.

We expect a similar behavior for the processes involving guanine crystals; however, the uncertainty related to some reaction channels allows us to predict only a virtually instant achievement of steady concentrations where the thermodynamically most preferable species of guanine tautomers dominate.

Since the proposed kinetic approach is fully ab initio based, it can be used for simulation of a wide range of processes beyond nucleobase tautomerization. This approach can be applied to almost any set of reactions for which activation barriers can be calculated.

Acknowledgment. Support has been provided by Grant NSF EPSCoR 440900362427-02. We acknowledge the Mississippi Center for Supercomputer Research for the computational facilities. D.K. thanks Dr. Manoj Shukla and Dr. Devashis Majumdar for useful discussion of the work.

References and Notes

(1) Mathews, C. K.; van Holde, K. E.; Ahern, K. G. *Biochemistry*, 3rd ed.; Addison-Wesley Longman: San Francisco, 1999.
(2) Saenger, W. In *Principles of Nucleic Acid Structure*; Cantor, C. R., Ed.; Springer-Verlag: New York, 1984.
(3) Watson, J. D.; Crick, F. H. C. *Nature* **1953**, *171* (4361), 964.
(4) Danilov, V. I.; Anisimov, V. M.; Kurita, N.; Hovorun, D. *Chem. Phys. Lett.* **2005**, *412*, 285.
(5) Kwok, P. Y. *Annu. Rev. Genomics Hum. Genet.* **2001**, *2*, 235.
(6) Vignal, A.; Milan, D.; SanCristobal, M.; Eggen, A. *Genet., Sel., Evol.* **2002**, *34* (3), 275.
(7) Strazewski, P. *Nucleic Acids Res.* **1988**, *16*, 9377.
(8) Topal, M. B.; Fresco, J. R. *Nature* **1976**, *263*, 285.
(9) Szczesniak, M.; Szczepaniak, K.; Kwiatkowski, J. S.; KuBulat, K.; Person, W. B. *J. Am. Chem. Soc.* **1988**, *110*, 8319.
(10) Choi, M. Y.; Dong, F.; Miller, R. E. *Philos. Trans. R. Soc. London, A* **2005**, *363*, 393.
(11) Choi, M. Y.; Miller, R. E. *J. Am. Chem. Soc.* **2006**, *128*, 7320.
(12) Nir, E.; Muller, M.; Grace, L. I.; de Vries, M. S. *Chem. Phys. Lett.* **2002**, *355*, 59.
(13) Nir, E.; Hünig, I.; Kleinermanns, K.; de Vries, M. S. *Phys. Chem. Chem. Phys.* **2003**, *5*, 4780.
(14) Nir, E.; Plützer, Ch.; Kleinermanns, K.; de Vries, M. *Eur. Phys. J. D* **2002**, *20* (3), 317.
(15) Mons, M.; Dimicoli, I.; Piuzzi, F.; Tardivel, B.; Elhanine, M. *J. Phys. Chem. A* **2002**, *106* (20), 5088.
(16) Mons, M.; Piuzzi, F.; Dimicoli, I.; Gorb, L.; Leszczynski, J. *J. Phys. Chem. A* **2006**, *110*, 38.
(17) Gorb, L.; Leszczynski, J. *J. Am. Chem. Soc.* **1998**, *120*, 5024.
(18) Gorb, L.; Kaczmarek, A.; Gorb, A.; Sadlej, A. J.; Leszczynski, J. *J. Phys. Chem. B* **2005**, *109*, 13770.
(19) Gorb, L.; Podolyan, Y.; Dziekonski, P.; Sokalski, W. A.; Leszczynski, J. *J. Am. Chem. Soc.* **2004**, *126*, 10119.
(20) Shukla, M. K.; Leszczynski, J. *Chem. Phys. Lett.* **2006**, *429*, 261.
(21) Hanus, M.; Ryjacek, F.; Kabelac, M.; Kubar, T.; Bogdan, T. V.; Trygubenko, S. A.; Hobza, P. *J. Am. Chem. Soc.;* **2003**, *125* (25), 7678.
(22) Kosenkov, D.; Gorb, L.; Shishkin, O. V.; Šponer, J.; Leszczynski, J. *J. Phys. Chem. B* **2008**, *112* (1), 150.
(23) Šponer, J.; Hobza, P. *J. Phys. Chem.* **1994**, *98*, 3161.
(24) Šponer, J.; Florian, J.; Hobza, P.; Leszczynski, J. *J. Biomol. Struct. Dyn.* **1996**, *13*, 827.
(25) Šponer, J.; Šponer, J. E.; Gorb, L.; Leszczynski, J.; Lippert, B. *J. Phys. Chem. A* **1999**, *103*, 11406.
(26) Yang, Z.; Rogers, M. T. *Phys. Chem. Chem. Phys.* **2004**, *6*, 2749.
(27) Pugliesi, I.; Muller-Dethlefs, K. *J. Phys. Chem. A* **2006**, *110* (48), 13045.
(28) Hui, C.; Shuhua, L. *J. Chem. Phys.* **2006**, *124*, 154315.
(29) Barbatti, M.; Lischka, H. *J. Am. Chem. Soc.* **2008**, *130* (21), 6831.
(30) Marian, C. M. *J. Phys. Chem. A* **2007**, *111*, 1545.
(31) de Vries, M. Two step laser mass spectrometry of polymers. In *Mass Spectrometry of Polymers*; Montaudo, G., Latimer, R. P., Eds.; CRC Press: Boca Raton, FL, 2001.
(32) Hall, R. B. *J. Phys. Chem.* **1987**, *91* (5), 1007.
(33) Zhao, Y.; Truhlar, D. G. *J. Phys. Chem. A* **2004**, *108*, 6908.
(34) Dunning, T. H. *J. Chem. Phys.* **1989**, *90*, 1007.
(35) Frisch, M. J.; Trucks, G. W.; Schlegel, H. B.; Scuseria, G. E.; Robb, M. A.; Cheeseman, J. R. ; Montgomery J. A., Jr.; Vreven, T.; Kudin, K. N.; Burant, J. C.; Millam, J. M.; Iyengar, S. S.; Tomasi, J.; Barone, V.; Mennucci, B.; Cossi, M.; Scalmani, G.; Rega, N.; Petersson, G. A.; Nakatsuji, H.; Hada, M.; Ehara, M.; Toyota, K.; Fukuda, R.; Hasegawa, J.; Ishida, M.; Nakajima, T.; Honda, Y.; Kitao, O.; Nakai, H.; Klene, M.; Li, X.; Knox, J. E.; Hratchian, H. P.; Cross, J. B.; Bakken, V.; Adamo, C.; Jaramillo, J.; Gomperts, R.; Stratmann, R. E.; Yazyev, O.; Austin, A. J.; Cammi, R.; Pomelli, C.; Ochterski, J. W.; Ayala, P. Y.; Morokuma, K.; Voth, G. A.; Salvador, P.; Dannenberg, J. J.; Zakrzewski, V. G.; Dapprich, S.; Daniels, A. D.; Strain, M. C.; Farkas, O.; Malick, D. K.; Rabuck, A. D.; Raghavachari, K.; Foresman, J. B.; Ortiz, J. V.; Cui, Q.; Baboul, A. G.; Clifford, S.; Cioslowski, J.; Stefanov, B. B.; Liu, G.; Liashenko, A.; Piskorz, P.; Komaromi, I.; Martin, R. L.; Fox, D. J.; Keith, T.; Al.Laham, M. A.; Peng, C. Y.; Nanayakkara, A.; Challacombe, M.; Gill, P. M. W.; Johnson, B.; Chen, W.; Wong, M. W.; Gonzalez, C.; Pople, J. A. Gaussian, Inc., Wallingford, CT, 2004.
(36) Kosenkov, D. Kinetic Simulation (kTSim) Program, http://www.ktsim.org.
(37) Eyring, H.; Walter, J.; Kimball, G. *Quantum Chemistry*; John Wiley and Sons: New York, London, Sydney, 1944.
(38) Press, W. H.; Flannery, B. P.; Teukolsky, S. A.; Vetterling, W. T. *Numerical Recipes in C*; Cambridge University Press: Cambridge, U.K., 1988.
(39) Kutta, M. W. *Z. Math. Phys.* **1901**, *46*, 435.
(40) Runge, C. *Math. Ann.* **1895**, *46*, 167.
(41) Dormand, J. R.; Prince, P. J. *J. Comput. Appl. Math.* **1980**, *6* (1), 19.
(42) Barker, D. L.; Marsh, R. E. *Acta Crystallogr.* **1964**, *17*, 1581.
(43) Thewalt, U.; Bugg, C. E.; Marsh, R. E. *Acta Crystallogr., B* **1971**, *27*, 2358.
(44) Guille, K.; Clegg, W. *Acta Crystallogr., C* **2006**, *62*, 515.
(45) Nir, E.; Janzen, C.; Imhof, P.; Kleinermanns, K.; de Vries, M. S. *Phys. Chem. Chem. Phys.* **2002**, *4*, 740.
(46) Fogarasi, G. *J. Phys. Chem. A* **2002**, *106* (7), 1381.
(47) Bell, R. L.; Taveras, D. L.; Truong, T. N.; Simons, J. *Int. J. Quantum Chem.* **1997**, *63* (4), 861.
(48) Zhao, Y.; Gonzaìlez-Garda, N.; Truhlar, D. G. *J. Phys. Chem. A* **2005**, *109* (9), 2012.

JP810570W